

## Low-Valent Complexes

How to cite: *Angew. Chem. Int. Ed.* **2023**, 62, e202218141

International Edition: doi.org/10.1002/anie.202218141

German Edition: doi.org/10.1002/ange.202218141

**Cationic Tetrylene-Iron(0) Complexes: Access Points for Cooperative, Reversible Bond Activation and Open-Shell Iron(-I) Ferrato-Tetrylenes\*\****Philip M. Keil, Ademola Soyemi, Kilian Weisser, Tibor Szilvási, Christian Limberg, and Terrance J. Hadlington\**

**Abstract:** The open-shell cationic stannylene-iron(0) complex **4** ( $4 = [\text{P}^{\text{PhIP}}\text{DippSn-Fe-IPr}]^+$ ;  $\text{P}^{\text{PhIP}}\text{Dipp} = \{[\text{Ph}_2\text{PCH}_2\text{Si}(\text{Pr})_2](\text{Dipp})\text{N}\}$ ;  $\text{Dipp} = 2,6\text{-Pr}_2\text{C}_6\text{H}_3$ ;  $\text{IPr} = [(\text{Dipp})\text{NC}(\text{H})_2\text{C}]$ ) cooperatively and reversibly cleaves dihydrogen at the Sn–Fe interface under mild conditions (1.5 bar, 298 K), in forming bridging hydrido-complex **6**. The One-electron oreduction of the related  $\text{Ge}^{\text{II}}\text{-Fe}^0$  complex **3** leads to oxidative addition of one C–P linkage of the  $\text{P}^{\text{PhIP}}\text{Dipp}$  ligand in an intermediary  $\text{Fe}^{-1}$  complex, leading to  $\text{Fe}^{\text{I}}$  phosphide species **7**. One-electron reduction reaction of **4** gives access to the iron(–I) ferrato-stannylene, **8**, giving evidence for the transient formation of such a species in the reduction of **3**. The covalently bound tin(II)-iron(–I) compound **8** has been characterised through EPR spectroscopy, SQUID magnetometry, and supporting computational analysis, which strongly indicate a high localization of electron spin density at  $\text{Fe}^{-1}$  in this unique  $d^9$ -iron complex.

## Introduction

The seminal discovery of stable carbene complexes by E. O. Fischer marked a turning point in modern organometallic chemistry,<sup>[1]</sup> our broader interest in the reactive capacity of carbene ligands blossoming since that time.<sup>[2]</sup> Extending from earlier concepts, bespoke pincer ligands incorporating nucleophilic carbene centers have the capacity to actively partake in cooperative bond scission processes across the carbene metal linkage,<sup>[3]</sup> in some cases reversibly.<sup>[4]</sup> Moving beyond the lightest element of group 14, the heavier tetrylenes also have the capacity to behave in this manner.<sup>[5]</sup> The past two decades have seen a significant growth in interest regarding the electronic nature of low-valent group 14 species,<sup>[6]</sup> and their bonding interactions with transition metals.<sup>[5,7]</sup> Due to the greater stability of lower oxidation states and the decrease in electronegativity on descending

group 14, their chemistry also deviates from that for carbon. Notably, the heavier tetrylenes have an amplified ambiphilicity, and are more Lewis acidic due to a lessened electro-negativity. This allows such ligands to behave as electrophiles whilst simultaneously being strong  $\sigma$ -donors towards a transition metal,<sup>[8]</sup> opening up a new vista in non-innocent ligand design (Figure 1).

Non-innocent ligand systems have been central in accessing challenging bond activation processes with the abundant first-row transition metals, notably so for iron.<sup>[9]</sup> Two-electron oxidative addition processes, key in classic cross-coupling reactions, are in fact quite uncommon for this abundant element,<sup>[10]</sup> with key methods which have enabled such processes at iron revolving almost exclusively around ligand design.<sup>[11]</sup> Utilizing chemically or redox non-innocent organic ligand systems, well-defined oxidative addition of catalytically essential bonds such as C–C, C–X ( $X = \text{Cl-I}$ ),<sup>[10]</sup> and H–H<sup>[12]</sup> bonds have been realized. In order to further expand accessibility to such key processes, our own research looks towards the development of non-innocent ligands based upon heavier low-valent group 14 elements. In this regard, heavier group 14-iron chemistry certainly has precedent. A small number of base-free silylene,<sup>[13]</sup> germylene,<sup>[14]</sup> and stannylene<sup>[14,15]</sup> complexes of iron(0) are now known, although it is noted that the vast majority involve the  $[\text{Fe}(\text{CO})_4]$  fragment or derivatives thereof, rendering reactivity involving the iron centre essentially nil. Closely related ferrato-tetrylenes have also seen considerable attention, exclusively featuring iron in the oxidation state –2. Here, base-free derivatives bearing two-coordinate group 14 centers are also rare, based largely on the monoanionic  $[\text{CpFe}(\text{CO})_2]^-$  fragment ( $\text{Cp} = \eta^5\text{-[C}_5\text{H}_5\text{]}^-$ ).<sup>[16]</sup> One very recent report on unique binding modes in ferrato-stannylene systems featuring the  $[\text{Cp}^*(\text{Pr}_2\text{MeP})\text{Fe}]$  ( $\text{Cp}^* =$

[\*] P. M. Keil, Dr. T. J. Hadlington  
Fakultät für Chemie, Technische Universität München  
Lichtenberg Strasse 4, 85747 Garching (Germany)  
E-mail: terrance.hadlington@tum.de

A. Soyemi, Prof. T. Szilvási  
Department of Chemical and Biological Engineering, University of Alabama  
Tuscaloosa, AL 35487 (USA)

K. Weisser, Prof. C. Limberg  
Institut für Chemie, Humboldt-Universität zu Berlin  
Brook-Taylor-Strasse 2, 12489 Berlin (Germany)

[\*\*] A previous version of this manuscript has been deposited on a preprint server (<https://doi.org/10.26434/chemrxiv-2022-7cztck>).

© 2023 The Authors. Angewandte Chemie International Edition published by Wiley-VCH GmbH. This is an open access article under the terms of the Creative Commons Attribution Non-Commercial NoDerivs License, which permits use and distribution in any medium, provided the original work is properly cited, the use is non-commercial and no modifications or adaptations are made.

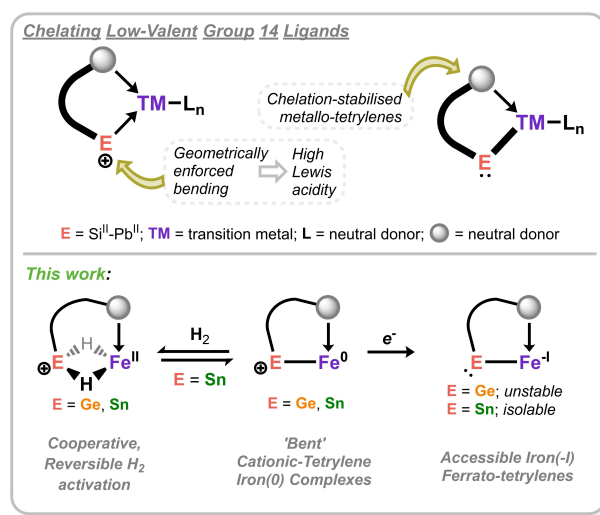


**Figure 1.** Above: Concepts in developing chelating low-valent group 14 systems, for geometrically activated ligand Lewis acidity, and stabilisation of otherwise inaccessible low-valent complexes. Below: this work involving chelating low-valent group 14 ligands in low-valent iron chemistry.

$\eta^5\text{-}[\text{C}_5\text{Me}_5]^-$ ) anionic fragment have been reported by Tilley et al.,<sup>[17]</sup> whilst a  $\text{Rh}^-$  metallo-stannylenes recently reported by Wesemann et al. was shown to activate  $\text{H}_2$  in the formation of a  $\text{Rh}^+$  metallo-stannylenes,<sup>[18]</sup> though a mechanistic investigation into the involvement of the  $\text{Sn}^{\text{II}}$  center was not disclosed.

Our own efforts have focused on the development of chelating ligands featuring a tetrylene binding center, which remains highly Lewis acidic even when bound to a transition metal due to chelation-induced geometric constraints (Figure 1).<sup>[8,19]</sup> This aims to exploit the tetrylene centre as an additional reactive site, to allow for tetrylene-transition metal cooperativity in bond activation. We also hypothesised that such a chelating ligand may give access to unique examples of metallo-tetrylenes, due to the strong stabilising nature of the chelate effect. Herein we describe the extension of our reported cationic  $\text{Ge}^{\text{II}}$  and  $\text{Sn}^{\text{II}}$  ligand systems to low-valent iron chemistry, in the facile “one-pot” synthesis of cationic germylene and stannylenes complexes of iron(0). The resulting systems are electronically distinct, the  $\text{Sn}^{\text{II}}$  complex having an open-shell ground state which allows for the facile and reversible activation of dihydrogen, the mechanism for which involves both the  $\text{Sn}^{\text{II}}$  and  $\text{Fe}^0$  centers in the critical H–H bond activation step. These complexes are also convenient access points for hitherto unknown open-shell ferrato-tetrylenes featuring  $\text{Fe}^{-1}$  centers. Whilst the target germanium system is unstable relative to ligand activation, the tin congener can be isolated as a stable, crystalline solid, which represents an open-shell, ferrato-stannylenes featuring a  $\text{Fe}^{-1}\text{-Sn}^{\text{II}}$  covalent bond.

## Results and Discussion

### Cationic Tetrylene- $\text{Fe}^0$ Complexes

Two-coordinate-tetrylene complexes of first-row transition metals are, as mentioned, uncommon.<sup>[13,14,15]</sup> Furthermore, almost all low-valent group 14-iron complexes employ carbonyl ligands at iron, leading to electronic saturation and thus diminished reactivity.

Our earlier reports regarding the synthesis of reactive  $\text{Ni}^0$  systems bearing our cationic tetrylene ligands relied upon the use of the commonly employed  $\text{Ni}^0$  synthon,  $\text{Ni}(\text{cod})_2$ . Earlier reports on similar chemistry for  $\text{Fe}^0$  systems utilized the elegant, but somewhat inaccessible metal-vapor synthesis of bis( $\eta^6$ -toluene)iron(0), used to generate the thermally labile ( $\eta^6$ -toluene)( $\eta^2$ -ethene)iron(0) complex.<sup>[15]</sup> More recently, a handful of closely related bis- $\eta^2$ -alkene  $\text{Fe}^0$  complexes were reported,<sup>[20]</sup> stabilized by bulky N-heterocyclic carbenes, which we believed may also readily undergo alkene substitution reactions.<sup>[21]</sup> To this end, the addition of the cationic  $\text{E}^{\text{II}}$  ligand precursors,  $[\text{P}^{\text{hiP}}\text{DippE}][\text{BAr}^{\text{F}}_4]$  ( $\text{E} = \text{Ge}$  (1),  $\text{Sn}$  (2);  $\text{P}^{\text{hiP}}\text{Dipp} = \{[\text{Ph}_2\text{PCH}_2\text{Si}(\text{Pr})_2](\text{Dipp})\text{N}\}$ ;  $\text{Dipp} = 2,6\text{-i-Pr}_2\text{C}_6\text{H}_3$ ;  $\text{Ar}^{\text{F}} = 3,5\text{-(CF}_3)_2\text{C}_6\text{H}_3$ ),<sup>[22,23]</sup> to deep green solutions of  $\text{IPr-Fe}[\eta^2\text{-(vtms)}]_2$  ( $\text{IPr} = [(\text{Dipp})\text{NC}(\text{H})_2\text{C}]$ ;  $\text{vtms} = \text{C}_2\text{H}_3\text{SiMe}_3$ ) rapidly led to the formation of deep yellow-brown reaction mixtures (Figure 2). In situ  $^{31}\text{P}\{^1\text{H}\}$  NMR spectroscopic

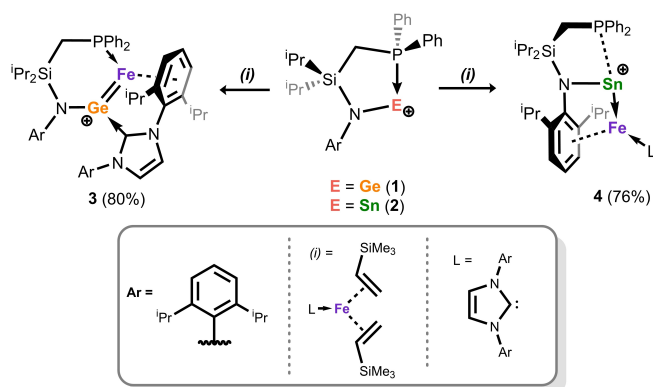


**Figure 2.** Synthesis of compounds **3** and **4** (isolated yields in parentheses); (i):  $\text{IPr-Fe}[\eta^2\text{-(vtms)}]_2$ , toluene, RT. Only the cationic part is shown in molecular structures. In all cases the counter-anion is  $[\text{BAr}^{\text{F}}_4]^-$  ( $\text{Ar}^{\text{F}} = 3,5\text{-CF}_3\text{C}_6\text{H}_3$ ).

analysis already suggested differing outcomes for the two reactions, that for the  $\text{Ge}^{\text{II}}$  system indicative of a single diamagnetic reaction product, and that for the  $\text{Sn}^{\text{II}}$  system being silent, thus indicative of a paramagnetic reaction product. Isolation of crystalline material from the two reaction mixtures (**3**: 80%; **4**: 76%) revealed considerably different structures for the two ligand systems.

The sole reaction product formed utilising the  $\text{Ge}^{\text{II}}$  ligand system (*viz.* **3**) shows  $\text{Fe}^0$  insertion into the Ge–P bond, forming our previously observed chelating ligand motif (Figure 3(a)).<sup>[24]</sup> However, presumably due to the high Lewis acidity of the cationic  $\text{Ge}^{\text{II}}$  centre, the NHC ligand has migrated from iron to germanium, the iron centre now forming an  $\eta^6$ -arene interaction with one Dipp group of this NHC ligand. The Ge–Fe distance in **3** ( $d_{\text{Ge-Fe}} = 2.1978$  (6) Å) is shorter than all but one reported Ge–Fe interactions, the one shorter example being found in a remarkable (alkyl)-(hydrido)germylene iron(II) complex.<sup>[14]</sup> The  $\text{Ge}^{\text{II}}$  center in **3** has a perfectly planar coordination geometry (sum of angles =  $359.8^\circ$ ), representative of a Ge→Fe dative interaction. The DFT derived HOMO (−9.16 eV; Figure S61 in Supporting Information) shows considerable  $\pi$ -character, which would suggest a degree of Fe→Ge back-bonding in this interaction and some degree of multiple-bond character. This is further borne out by both the Mayer Bond Order (MBO) and Wiberg Bond Index (WBI) for this bond, at 1.37 and 1.35, respectively, as calculated for model complex **3'** (**3'** =  $[\text{Me}^{\text{Mc}}\text{XylGe-Fe-PhNHC}]^+$ ;  $\text{Me}^{\text{Mc}}\text{Xyl} = \{[\text{Me}_2\text{PCH}_2\text{SiMe}_2\text{-}(\text{Xyl})\text{N}\}$ ;  $\text{Xyl} = 2,6\text{-Me}_2\text{C}_6\text{H}_3$ ;  $\text{PhNHC} = [(\text{Ph})\text{NC}(\text{H})_2\text{C}]$ ). The average of the C–C bond lengths in the Fe-bound arene ( $d = 1.419$  Å) is slightly greater than the same value for the unbound arene of the NHC ligand ( $d = 1.390$  Å), as is known in related arene complexes of low-valent iron.<sup>[25]</sup> Considerable broadening of aliphatic signals in the  $^1\text{H}$  NMR spectrum of **3** indicates a fluxional character in solution, which sharpen when THF- $d_8$  solutions are heated to  $60^\circ\text{C}$  (Figure S5 in Supporting Information). Notably, at low temperature (*i.e.*  $-80^\circ\text{C}$ ) clear signals at  $\delta = 4.5$ , 5.4, and 6.5 ppm can be seen, pertaining to the Fe-bound Dipp group.<sup>[26]</sup> The  $^{57}\text{Fe}$  Mössbauer spectrum of **3** ( $\delta =$

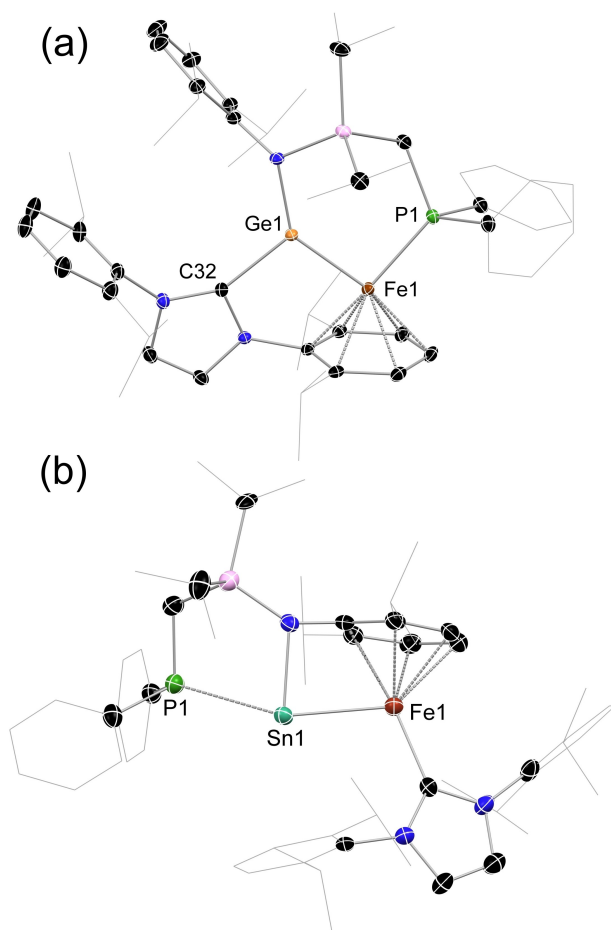


**Figure 3.** Molecular structure of the cationic parts in (a) **3** and (b) **4**, with thermal ellipsoids at 25% probability, and hydrogen atoms omitted for clarity. Selected bond length (Å) and angles (°) for **3**: Ge1–Fe1 2.1978(6); Ge1–C32 2.049(2); Ge1–N1 1.845(2); P1–Fe1 2.2109(9); N1–Ge1–Fe1 137.75(6); N1–Ge1–C32 119.77(7); Fe1–Ge1–C32 102.28(6); Ge1–Fe1–P1 94.17(3). For **4**: Sn1–Fe1 2.717(1); P1–Sn1 2.998(2); Fe1–C32 2.073(5); Sn1–N1 2.140(3); C1–N1 1.396(7).

$0.472 \text{ mm s}^{-1}$ ;  $\Delta E_{\text{O}} = 1.349 \text{ mm s}^{-1}$ ; Figure S48 in Supporting Information) is in keeping with known  $\text{Fe}^0$  arene systems,<sup>[24]</sup> aiding in confirmation of a low-spin,  $d^8 \text{ Fe}^0$  complex. This species, to the best of our knowledge, thus represents a unique example of a cationic-tetrylene  $\text{Fe}^0$  complex, and the first  $\text{Ge}^{\text{II}}\text{--Fe}^0$  complex absent of carbonyl ligands. The structural and electronic nature of the closely related  $\text{Sn}^{\text{II}}$  system, **4** (Figure 3), contrasts that of the described  $\text{Ge}^{\text{II}}$  complex. The  $\text{Sn}^{\text{II}}$  center indeed binds the  $\text{Fe}^0$  center; surprisingly, however, insertion into the Sn–P bond is not observed, but rather the  $\text{Fe}^0$  center forms an  $\eta^6$ -arene interaction with the Dipp group of the stannylene ligand, generating a highly strained conformation. This strain presumably leads to a significant weakening of the P–Sn interaction, which is longer than 98% of reported Sn–P single-bonded interactions ( $d_{\text{Sn–P}} = 2.999(2) \text{ \AA}$ ; sum of covalent radii =  $2.51 \text{ \AA}$ ). The ligand strain is exemplified by the acute Sn–Fe binding angle ( $\angle_{\text{NSnFe}} = 81.32(1)^\circ$ ), and further borne out by the angles at the  $\text{Ph}^{\text{IP}}$ Dipp ligand's N–donor

atom: the Sn–N–C<sup>Dipp</sup> and Si–N–C<sup>Dipp</sup> angles of  $94.81(3)^\circ$  and  $142.61(3)^\circ$  deviate significantly from the ideal of  $120^\circ$ . Finally, the Sn–Fe bond length of  $2.717(1) \text{ \AA}$  is longer than all known terminal Sn–Fe bonding interactions. The low-coordinate  $\text{Sn}^{\text{II}}$  center appears to have some degree of stabilization from one aryl group of the NHC ligand bound to  $\text{Fe}^0$ , with a distance of  $3.316 \text{ \AA}$  between the  $\text{Sn}^{\text{II}}$  center and the center of the arene plane. This is within the sum of the van der Waals radii for tin and carbon ( $3.97 \text{ \AA}$ ),<sup>[27]</sup> but considerably longer than such interactions in related low-coordinate tetrylene cations.<sup>[28]</sup> Electronically,  $\text{Sn}^{\text{II}}$  complex **4** also differs to the  $\text{Ge}^{\text{II}}$  system. Solutions of redissolved crystalline **4** yield highly broadened  $^1\text{H}$  NMR spectra, indicative of a paramagnetic system. This paramagnetism is rationalized best assuming a high-spin configuration for the  $d^8 \text{ Fe}^0$  center, with  $S=1$ . Consistent with this, complex **4** is not active when studied by X-band EPR spectroscopy, and shows the expected behavior for an  $S=1$  system in SQUID magnetometry measurements (Figure 4). Here, the ambient temperature  $\mu_{\text{eff}}$  value of  $3.95 \mu_{\text{B}}$  is higher than would be expected for the spin-only value for two unpaired electrons (e.g.  $2.83 \mu_{\text{B}}$ ), indicative of spin-orbit coupling, which is known for heavier group 14 element first-row transition metal complexes.<sup>[29]</sup> These SQUID data are also in good agreement with Curie-Weiss paramagnetism, indicative of

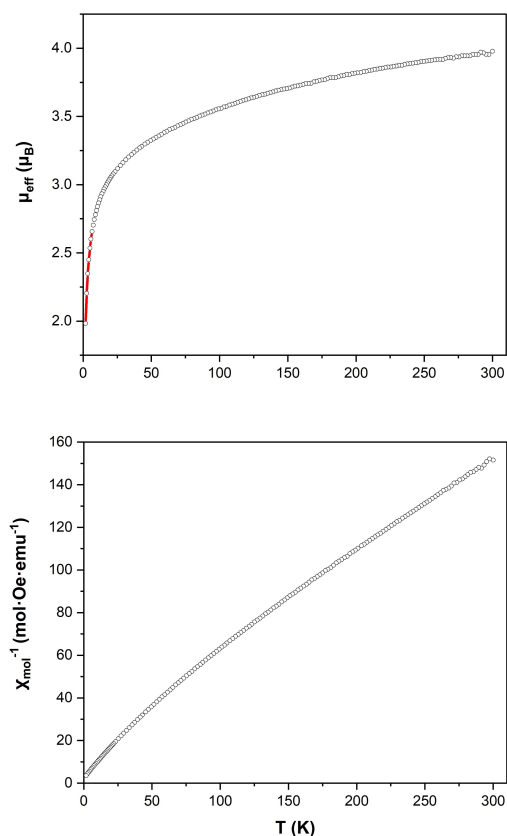


**Figure 4.** Plots of  $\mu_{\text{eff}}$  vs.  $T$  (above) and  $\chi_{\text{mol}}$  vs.  $T$  (below) for paramagnetic  $\text{Sn}^{\text{II}}\text{--Fe}^0$  complex **4**.

spin-density located at iron, with no indication of spin-coupling e.g. arising from ligand reduction. Density Functional Theory (DFT) calculations on model complex **4'** (**4'** =  $[\text{MeMeXylSn-Fe}^{\text{Xyl}}\text{NHC}]^+$ ;  $\text{XylNHC} = [(\text{Xyl})\text{NC}(\text{H})_2\text{C}]$ ) also suggest a high spin density at iron (Figure S64 in Supporting Information). Notably, this spin state leads to a very narrow calculated HOMO-LUMO gap in **4'** of 0.89 eV.<sup>[30]</sup> Alongside the geometrically perturbed Sn-Fe interaction and low-coordination environment at the cationic Sn<sup>II</sup> center, this provides a promising platform for synergistic bond activation in this complex.

### Cooperative bond activation

The differing electronic nature of the described complexes stands as an exciting point of comparison, exemplified by their reactivity. One of our key aims in the development of ambiphilic main group ligands (e.g. **1** and **2**) seeks to access systems whereby the ambiphilic ligand has the capacity to bind incoming nucleophiles, with a focus on ammonia.<sup>[31]</sup> This aims to activate ammonia in the coordination sphere of the transition metals, which is typically a highly challenging reaction.<sup>[32]</sup> Both complexes **3** and **4** rapidly react with ammonia. Addition of  $\approx 1.5$  equiv of ammonia to dissolved **3** led to dissipation of its characteristic deep golden-yellow color, and formation of deep red solutions. In situ <sup>1</sup>H and

<sup>31</sup>P{<sup>1</sup>H} NMR spectroscopic analysis indicated the clean formation of a single reaction product, with a broad 2H singlet in the <sup>1</sup>H NMR spectrum attributable to an NH<sub>2</sub> moiety ( $\delta = 2.26$  ppm). In contrast, the same reaction for the Sn<sup>II</sup> system **4** led instead to a complex mixture of products,<sup>[33]</sup> highlighting differences in the reactivity of these distinct iron-tetrylene species. Deep red single crystals isolated from the former reaction indicated the activation of ammonia, through binding at Ge<sup>II</sup>, and proton transfer to the NHC ligand, in the formation of **5** (Figure 5), in 93% isolated yield. This thus indicates that the Ge<sup>II</sup> center in **4** is indeed of high Lewis acidity, and so capable of binding the incoming nucleophilic NH<sub>3</sub>. Compound **5** represents a rare example of a “half-parent” amido tetrylene-transition metal complex,<sup>[34]</sup> and the first such example for germanium. Remarkably, the now protonated imidazolium salt remains bound to the Fe<sup>0</sup> center through an  $\eta^6$ -arene interaction. The Ge-Fe distance of 2.219(1) Å is slightly elongated relative to starting material **3**, likely due to increased N→Ge donation, so reducing Fe→Ge back-bonding. As described, the NH<sub>2</sub> ligand at Ge can be observed in the <sup>1</sup>H NMR spectrum ( $\delta = 2.26$  ppm), as well as in the IR spectrum of the powdered compound ( $\nu = 3434$  and  $3335$  cm<sup>-1</sup>). Despite the persistent binding of the protonated NHC in **5**, attempts to drive reversibility in this ammonia activation reaction failed, e.g. through application of heat and/or vacuum to dissolved **5**. Still, this reaction demonstrates a unique cooperative

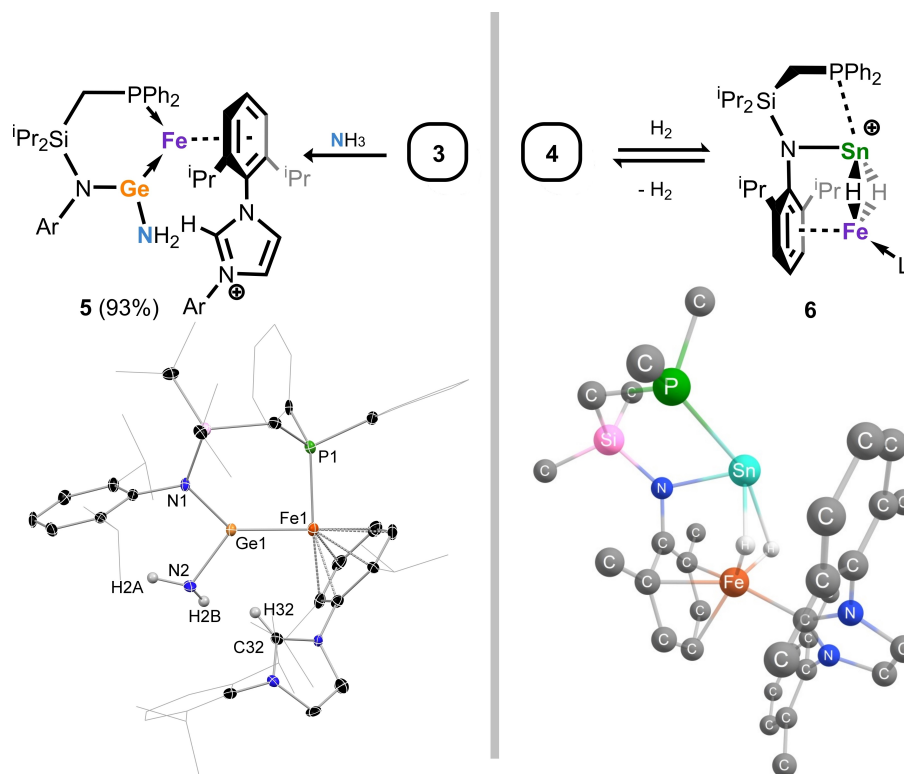


**Figure 5.** Above: the reactivity of **3** and **4** towards NH<sub>3</sub> and H<sub>2</sub>, respectively, showing reversibility in the latter. Below: the molecular structure of the cationic part in NH<sub>3</sub>-activation product **5**, with thermal ellipsoids at 25% probability, and the DFT-derived structure of the cationic part in H<sub>2</sub> activation product **6**. Selected bond length (Å) and angles (°) for **5**: Ge1-Fe1 2.219(1); Ge1-N1 1.853(5); Ge1-N2 1.870(7); Fe1-P1 2.210(3); Ge1...C32 3.520(9); N1-Ge1-N2 98.8(3); Fe1-Ge1-N1 136.2(2); Fe1-Ge1-N2 124.8(2).

ammonia activation mechanism, in which the low-valent group 14 element (e.g. Ge<sup>II</sup>) interestingly maintains its low oxidation state.

We then moved our sights to the activation of H<sub>2</sub>, expected to be more challenging given the nonpolar nature of this small molecule. Here, Ge<sup>II</sup> complex **3** showed no signs of reactivity, even after prolonged heating and increased H<sub>2</sub> pressures (e.g. up to 3 bar). Complex **4**, on the other hand, readily reacts with H<sub>2</sub> under 1.5 bar pressure, and at ambient temperature. Charging a gas-tight NMR tube containing a C<sub>6</sub>D<sub>6</sub> solution of paramagnetic **4** with H<sub>2</sub> led to the formation of a single new diamagnetic reaction product, showing a singlet in the <sup>31</sup>P{<sup>1</sup>H} NMR spectrum at  $\delta = -24.2$  ppm. More poignantly, a broad signal is observed in the <sup>1</sup>H NMR spectrum, at  $\delta = -13.63$  ppm, integrating to 2H and bearing clear <sup>117/119</sup>Sn satellites (<sup>1</sup>J<sub>SnH</sub> = 331 Hz; Figure S18 in Supporting Information). Conducting the same reaction with D<sub>2</sub> gives a <sup>1</sup>H NMR spectrum identical to that described, but absent of the described high-field resonance (Figure S26 in Supporting Information). The <sup>2</sup>D NMR spectrum of these reaction mixtures reveals a resonance at  $\delta = -13.97$  ppm, in keeping with the activation of D<sub>2</sub> (Figure S28 in Supporting Information). Evidence that these oxidative addition reactions may be reversible was found on addition of D<sub>2</sub> to in situ generated **6**, which led to the formation of HD gas (Figure S39 in Supporting Information). Confirming this, degassing these reaction mixtures leads to quantitative regeneration of the starting material, thus signifying the facile reversible H<sub>2</sub> activation by **4**. This point rendered it highly challenging to attain further analytical data on this complex, and indeed to crystallize pure samples of H<sub>2</sub> activation product **6**. Although crystalline material of this species could be isolated by crystallising under an atmosphere of H<sub>2</sub>,<sup>[35]</sup> high levels of disorder prevented refinement to levels acceptable for publication; nevertheless, this did allow us to ascertain the connectivity in **6** (Figure S60 in Supporting Information). Furthermore, this data could be utilized for the computationally derived lowest energy conformation of model complex **6'** (**6'** = [<sup>MeMe</sup>XylSn(μ-H)<sub>2</sub>Fe<sup>Xyl</sup>NHC]<sup>+</sup>; Figure 5). Here, it is found that the hydride ligands in this complex symmetrically bridge the Sn and Fe centers, in keeping with the single resonance observed for these ligands in <sup>1</sup>H NMR spectra of reaction mixtures. Indeed, although rare, known examples of stannane-iron complexes featuring bridging hydride ligands have similar shifts and coupling constants in their respective <sup>1</sup>H NMR spectra.<sup>[36]</sup> At this stage, we were particularly curious as to whether the reversible activation of H<sub>2</sub> in **4** proceeds via a cooperative mechanism, that is, involving both Sn and Fe. A DFT investigation of the potential energy surface for this reaction mechanism suggests that this is indeed the case (Figure 6). Upon initial H<sub>2</sub> addition an intermediary  $\sigma$ -complex is formed at Fe<sup>0</sup> (IM1, 16.1 kcal mol<sup>-1</sup>). One H-atom can then form a bridging interaction with the cationic Sn<sup>II</sup> center (TS2, 21.2 kcal mol<sup>-1</sup>). This then proceeds by H–H bond scission, so forming bridging hydride complex **6** (–4.0 kcal mol<sup>-1</sup>). This reaction coordinate therefore incites the involvement of both Sn and Fe centres in the cleavage of H<sub>2</sub>, giving

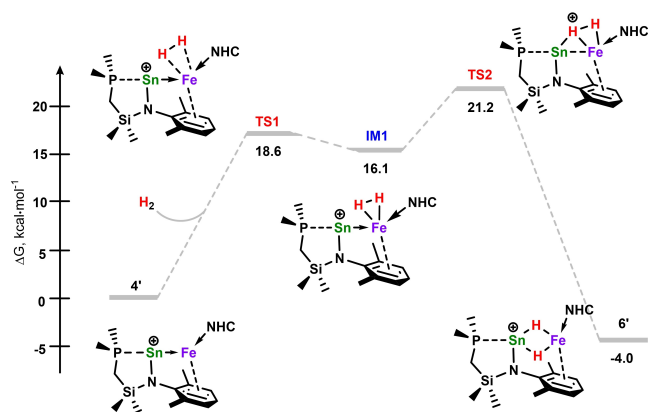
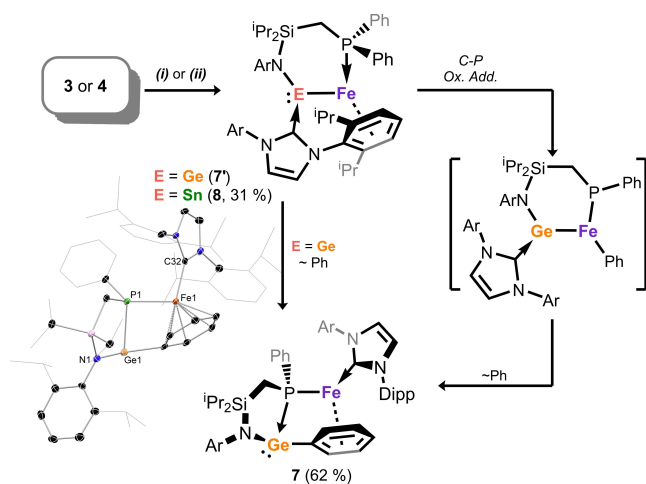


**Figure 6.** The DFT-derived reaction coordinate for the cooperative activation of H<sub>2</sub> by model cationic stannylene-iron(0) complex **4'**, yielding **6'**.

insights into the design of heteroelemental systems for the cooperative activation of typically nonlabile bonds. The small exergonic value for the overall reaction (4.0 kcal mol<sup>-1</sup>) is in keeping with the observed reversibility in this process. An additionally important point here is the oxidation state of iron in the formed hydride complex. Combined X-ray crystallographic studies and DFT calculations indicate a *pseudo*-octahedral iron centre in **6**. This, in addition to the diamagnetic nature of this compound, would indicate a low-spin d<sup>6</sup> Fe<sup>II</sup> electronic configuration, indicative of a two-electron oxidative addition at the iron centre in **4** upon H<sub>2</sub> addition.<sup>[10–12]</sup> This further highlights the utility of the novel cationic tetrylene ligands employed here, in assisting otherwise challenging bond activation processes.

#### Accessing Open-Shell Ferrato-Tetrylenes

Despite the low-valent nature of both the tetryl and transition elements in complexes **3** and **4**, we hypothesized that their reduction may be possible, given that sub-valent iron systems (*viz.* ferrates) are known.<sup>[37]</sup> The most common such species are Fe<sup>-II</sup> complexes, which are stable due to their d<sup>10</sup> electronic configuration.<sup>[33]</sup> On the other hand, formal d<sup>9</sup> Fe<sup>-I</sup> complexes are very rare indeed. This compound class is largely represented by ion-separated alkali metal ferrates, such as Ellis's [(η<sup>4</sup>-anth)<sub>2</sub>Fe][K(L)<sub>n</sub>].<sup>[33]</sup> A number of reduced complexes derived from or relating to this ferrate involving redox active ligands are indeed known, whereby ligand reduction occurs, forming higher valent iron species.<sup>[38]</sup> Further examples of salt-separated anionic complexes, potentially featuring Fe<sup>-I</sup> centers have been reported by Peters et al., although the oxidation state at iron is not entirely clear, with potential reduction of employed ligands (e.g. borane, dinitrogen, and/or cyclic-alkylaminocarbene).<sup>[39]</sup> Covalently bound Fe<sup>-I</sup> species remain elusive. In this regard, one-electron reduction of both **3** and **4** would lead to neutral ferrato-tetrylene complexes, featuring covalently bound, open-shell Fe<sup>-I</sup> centers (Scheme 1).



**Scheme 1.** Reduction of complexes **3** and **4**, forming ferrato-stannylene **8**, and ligand-activation product **7** (inset: molecular structure of **7**, with thermal ellipsoids at 25% probability); (i) Cp\*<sub>2</sub>Co, toluene, -40 °C-RT (E = Ge); (ii) IPr-Fe[η<sup>2</sup>-(vtms)]<sub>2</sub>, toluene, RT (E = Sn). Selected bond lengths (Å) and angles (°) for compound **7**: Ge1-P1 2.393(2); Ge1-N1 1.953(5); Fe1-P1 2.272(2); Fe1-C32 1.956(6); N1-Ge1-P1 92.1(1); P1-Ge1-C26 75.5(2); N1-Ge1-C26 105.8(2); C32-Fe1-P1 100.7(2); P1-Fe1-C26 76.7(2).

We first investigated the electrochemistry of complexes **3** and **4**, as THF solutions against the ferrocene reference electrode (Figure 7). Both complexes show chemically reversible reduction events (Ge:  $E_{1/2} = -1.65$  V; Sn:  $E_{1/2} = -1.44$  V).<sup>[40]</sup> Given that these values are roughly within the reduction potential of Cp\*<sub>2</sub>Co,<sup>[41]</sup> we sought the chemical one-electron reduction of both **3** and **4** with this soluble reducing agent. Reduction of the Ge<sup>II</sup> system led to formation of a deep red solution, with the precipitation of a pale yellow powder presumed to be [Cp\*<sub>2</sub>Co][BAR<sup>F</sup><sub>4</sub>]. Analysis of the reaction mixture by <sup>1</sup>H NMR spectroscopy revealed only highly broadened spectra indicative of paramagnetism in reaction products. Yields of up to 62% of a single reaction product could be isolated as deep red crystals, found to be the ligand activated product **7** (Scheme 1, inset), formally a phosphido-iron(I) compound. We hypothesise that this forms via an intermediary ferrato-germylene **7**, with an Fe<sup>-1</sup> centre, which oxidatively cleaves one P-Ph bond of the flanking ligand arm. Ph-migration from Fe to Ge generates the final (phenyl-germylene)iron-phosphide product (Scheme 1).<sup>[42]</sup> In such a case, this process would represent a further example of a formal two-electron oxidative addition involving iron, albeit at an Fe<sup>-1</sup> center. Structurally, complex **7** contains no formal Ge-Fe interaction ( $d_{\text{Ge-Fe}} = 3.432(2)$  Å); the NHC ligand has now migrated back to the iron(I) center, which also bears an η<sup>6</sup>-arene interaction with the phenyl moiety at Ge<sup>II</sup>.

Extending this chemistry to the Sn<sup>II</sup> system, we were surprised to find that in fact the tin congener of the target d<sup>9</sup> ferrato-tetrylene is indeed stable. Although reduction with Cp\*<sub>2</sub>Co also led to the formation of a yellow precipitate, again presumably [Cp\*<sub>2</sub>Co][BAR<sup>F</sup><sub>4</sub>], isolation of meaningful quantities of a pure product proved challenging from these

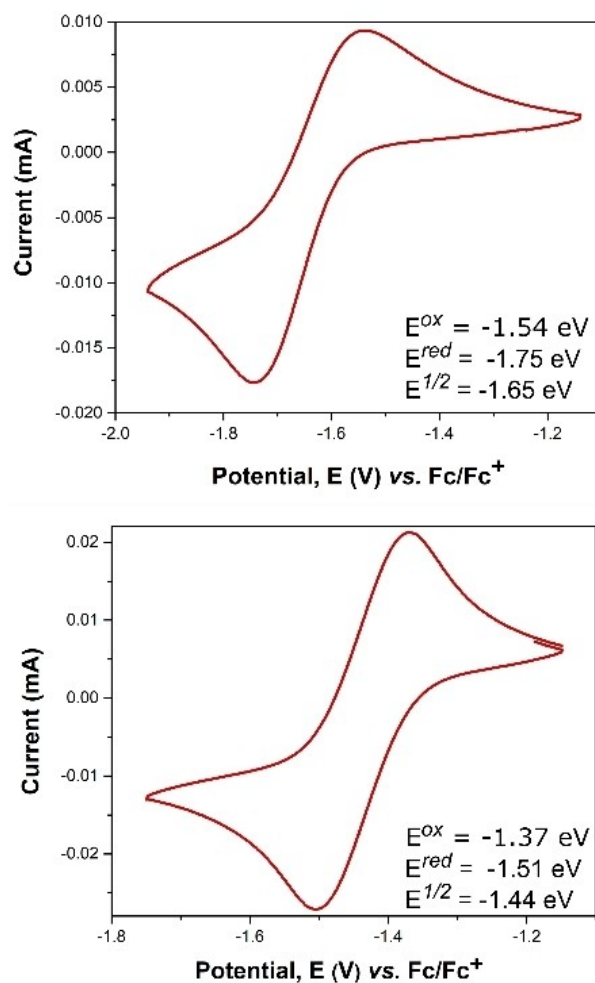


**Figure 7.** Cyclic voltammograms of complexes **3** (above) and **4** (below), in THF/[N(n-Bu)<sub>4</sub>]PF<sub>6</sub>, at a scan rate of 100 mV s<sup>-1</sup>.

reaction mixtures. However, direct addition of two equivalents of the Fe<sup>0</sup> synthon IPr-Fe[η<sup>2</sup>-(vtms)]<sub>2</sub> to the cationic stannylene **2** proved to be reducing enough to form the ferrato-stannylene **8** in crystalline yields of up to 31% (Scheme 1, Figure 8), with isolated yields being hindered by challenges in its separation from oily cationic by-products. The molecular structure of compound **8** is similar to that for the cationic germylene complex **3**, in that the ligand's phosphine arm now chelates the formally Fe<sup>-1</sup> center, and the NHC is now located on Sn<sup>II</sup>, with one Dipp fragment forming an η<sup>6</sup>-arene interaction with iron. The key difference is the coordination geometry at Sn<sup>II</sup>, which is now trigonal pyramidal due to the presence of a stereo-active lone pair of electrons (sum of angles = 309.76°). This contrasts with that of the Ge<sup>II</sup> center in **3**, the planarity of which indicates Ge→Fe electron donation (sum of angles = 359.8°), and thus the absence of a formal bonding interaction. A notable contraction of the Sn-Fe bond length is observed on moving from cationic **4** to neutral **8**, concomitant with a considerable decrease in the calculated polarization in this bond (Table 1). These observations point

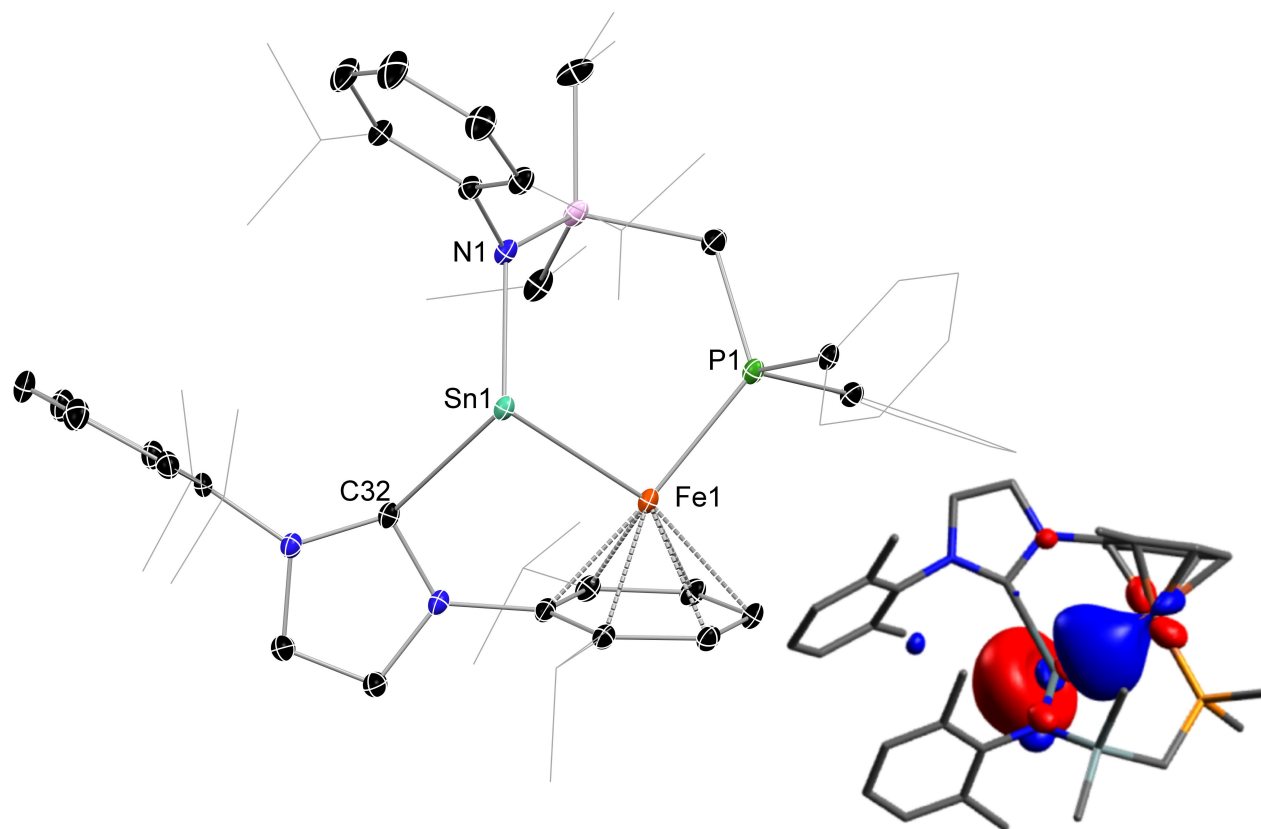


**Figure 8.** The molecular structure of iron(-I) ferrato-stannylene **8**, with ellipsoids at 25% probability, and hydrogen atoms omitted for clarity (inset: HOMO-1, representing the Sn-centered lone electron pair). Selected bond lengths (Å) and angles (°) for **8**: Sn1-Fe1 2.6489(9); P1-Fe1 2.238(1); Sn1-N1 2.186(2); Sn1-C32 2.444(3); Sn1-Fe1-P1 96.06(2); Fe1-Sn1-N1 107.59(6); Fe1-Sn1-C32 86.34(6); N1-Sn1-C32 115.44(8).

**Table 1:** Selected metrical, analytical, and calculated parameters for **4** and **8**.

		<b>4</b>	<b>8</b>
dSn-Fe, Å		2.717(1)	2.6489(9)
Mössbauer	Isomer Shift, $\delta$	0.777	0.520
	$\Delta E_Q$ , mm·s <sup>-1</sup>	1.349	1.574
Fe-Sn Bond	Fe/Sn	24.23/75.77	58.19/41.81
	Polarisation[a]		
Spin population, %[b]	Fe/Sn	70.97/11.13	77.95/16.36
NPA charge[a]	Sn/Fe/C	0.59/0.53/0.15	0.65/-0.19/1.02
WBI[a]	Sn-Fe/Fe-C	0.52/0.57	0.78/0.73
MBO[a]	Sn-Fe/Fe-C	0.53/0.77	0.82/0.80

[a] as determined through an NBO analysis of model complexes **4'** and **8'**; [b] as determined through spin-unrestricted DFT computations of model complexes **4'** and **8'**.

towards a formal covalent Sn-Fe bonding interaction in **8**. The absence of any other redox-active ligand bound to the Fe center in this complex would lead to the formal oxidation states of Sn<sup>II</sup>/Fe<sup>-1</sup>. The paramagnetic nature of **8**, ascertained by its <sup>1</sup>H NMR spectrum ( $\mu_{\text{eff}} = 2.38 \mu_B$  using Evans method), indicates that this species is indeed an example of an open-shell metallo-tetrylene. To the best of our knowledge this represents the first example of such a compound, and indeed a unique example of a covalently bound iron(-I) complex.

To gain further insights into the electronic nature of ferrato-stannylene **8**, and to ascertain the location of the free electron in this species, a combination of SQUID magnetometry, and EPR and Mössbauer spectroscopy were employed, supported by DFT calculations. The EPR spectrum of a frozen glass of **8** in toluene (5 mM) yields a rhombic spectrum (Figure 9).<sup>[43]</sup> Supported by the simulated spectrum, three g-values of 2.0126, 2.0410, and 2.3050 are found, giving a  $g_{\text{iso}}$  of 2.1195, fitting well for an iron-centered electron.<sup>[44]</sup> Hyperfine coupling to <sup>31</sup>P, <sup>117</sup>Sn, and <sup>119</sup>Sn is clearly observable, the scales of which also indicate negligible radical character at these centers (Table S10).<sup>[45]</sup> Calculated spin-density plots of model complex **8'** also infer a high degree of spin-density at Fe (77.95%; Figure 9). The zero-field <sup>57</sup>Fe Mössbauer spectrum of **8** exhibits an unsymmetrical quadrupole doublet with an isomer shift of  $\delta = 0.520 \text{ mm s}^{-1}$ , and a large quadrupole splitting of  $\Delta E_Q = 1.574 \text{ mm s}^{-1}$ . Although the isomer shift is typically considered a key parameter for the assignment of the oxidation state, the lack of reported Fe<sup>-1</sup> compounds limits the applicability of this tool in the present case, especially given that isomer shifts have also been found to depend on various other factors (ligand properties, ligation etc.).<sup>[46]</sup> In this regard, **8** is compared perhaps most reasonably with compound **3** ( $\delta = 0.472 \text{ mm s}^{-1}$ ;  $\Delta E_Q = 1.349 \text{ mm s}^{-1}$ ), which features a rather similar ligand scaffold around the iron

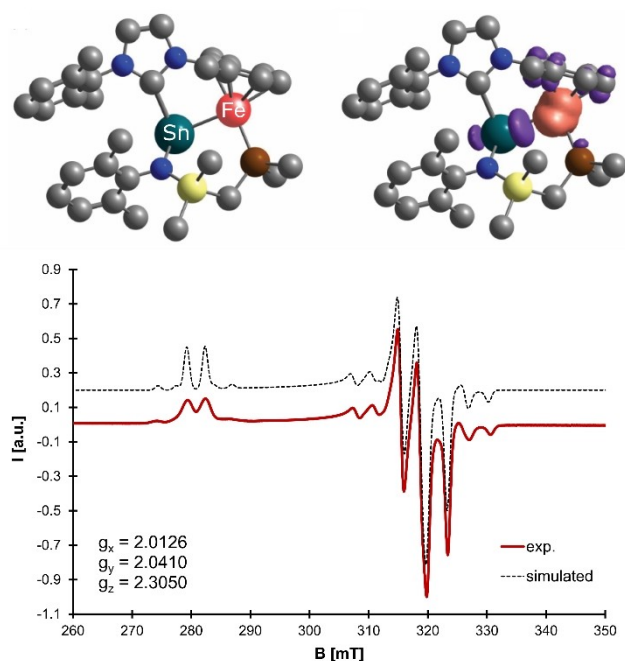


**Figure 9.** Above: the DFT optimized structure of **8**, and a spin-density plot of **8**, orange showing areas of positive density, and purple negative. Below: the EPR spectrum of **8** as a frozen THF glass at 113 K, overlaid with the simulated spectrum.

center. Lowering the oxidation state from  $\text{Fe}^0$  to  $\text{Fe}^{-1}$  on going from **3** to **8** would be expected to lead to a shift of the isomer shift into the positive region. The lengthening of the iron-tetryl element bond in **8** compared to that in **3** should also lead to a more positive isomer shift, which is indeed the case. However, even more factors change (replacement of Ge by softer Sn, and transformation of a dative bond into a covalent bond), so that it is advisable not to overinterpret these data. The same holds true for the quadrupole splitting that is comparable for both compounds. Looking now at magnetometry data, the inverse of  $\mu_{\text{eff}}$ , derived from SQUID measurements, shows a linear increase with increasing temperature (Figure S46 in Supporting Information), in keeping with Curie-Weiss magnetism, and again indicative of an iron-centered electron. The SQUID-derived magnetic moment for **8** ( $\mu_{\text{eff}}^{298} = 2.33 \mu_{\text{B}}$ ) is in keeping with that found in the solution state using the Evans method ( $2.38 \mu_{\text{B}}$ ), and is considerably lower than that observed for cationic complex **4** ( $3.95 \mu_{\text{B}}$ ), as is expected following a one electron reduction. Again, as for **4**, this is greater than the spin-only value expected for an  $S = 1/2$  system, indicative of spin-orbit coupling in this compound.<sup>[26]</sup> With these key data in hand, it is clear that **8** bears a single unpaired electron, which is localized at the iron center in this compound, demonstrated primarily through EPR spectroscopy, and supported by DFT studies. Thus, the data discussed here strongly support the formation of a molecular, covalent  $d^9 \text{Fe}^{-1}$  compound in **8**.

## Conclusion

We have presented facile synthetic routes for access to unprecedented cationic-tetrylene complexes of iron (0). Intrinsic differences in the electronic nature of the  $\text{Ge}^{\text{II}}$  and  $\text{Sn}^{\text{II}}$  ligands leads to considerably different electronic states in the formed complexes: the  $\text{Ge}^{\text{II}}$  system forms a low-spin, closed shell ground state, whilst the  $\text{Sn}^{\text{II}}$  complex has a high-spin, open shell ground state. The high reactivity of the latter open shell system is demonstrated through the activation of dihydrogen, a process which is in fact reversible, and proceeds via a cooperative mechanism involving both  $\text{Sn}^{\text{II}}$  and  $\text{Fe}^0$  in the key bond scission step. Further, the described tetrylene iron (0) complexes prove to be ideal synthons for accessing hitherto unknown iron (-I) ferrato tetrylenes. Whilst the germanium system is unstable, undergoing ligand activation presumably through a two-electron oxidative addition process at iron, the  $\text{Sn}^{\text{II}}\text{-Fe}^{-1}$  system is a stable, crystalline compound. Thorough analysis of this unique species suggests a high degree of spin density at Fe, and a highly covalent Sn-Fe bonding interaction, opening a new vista in low-valent *d*-block chemistry. Further expansion of this compound class is currently underway in our laboratories, to uncover the reactivity of these unprecedented species, with a focus on two-electron oxidative addition processes which are typically challenging in iron chemistry.

## Acknowledgements

T.J.H. thanks the Fonds der Chemischen Industrie (FCI) for generous funding of this research through a Liebig Stipendium, the DFG for an Independent Research grant (Project Nr. HA9030/3-1470323245), and the Technical University Munich for the generous endowment of TUM Junior Fellow Funds. We also thank M. Muhr, O. Storcheva, and I. Znakovskaya for the measurement of LIFDI-MS, EPR, and SQUID data, respectively, as well as L. Niederegger and K. Rickmeyer for help with CV measurements, and P. Coburger for modelling EPR data. T.S. thanks the University of Alabama and the Office of Information Technology for providing high performance computing resources and support. This computational work was made possible in part by a grant of high-performance computing resources and technical support from the Alabama Supercomputer Authority. C.L. is grateful to the cluster of excellence “Uni-SysCat” funded by the DFG under Germany’s Excellence Strategy-EXC2008/1-390540038. Open Access funding enabled and organized by Projekt DEAL.

## Conflict of Interest

The authors declare no conflict of interest.

## Data Availability Statement

Data available in article supplementary material, and additionally on request from the authors.

**Keywords:** Cationic Tetrylenes · Cooperative Bond Activation · Low-Valent Iron · Low-Valent Main Group · Sustainability

- [1] E. O. Fischer, A. Maasbøll, *Angew. Chem. Int. Ed. Engl.* **1964**, *3*, 580–581; *Angew. Chem.* **1964**, *76*, 645–645.
- [2] a) D. J. Cardin, D. Çetinkaya, M. F. Lappert, *Chem. Rev.* **1972**, *72*, 545–574; b) F. Glorius, *N-Heterocyclic Carbenes in Transition Metal Catalysis*, Springer, Berlin, Heidelberg, **2007**; c) F. E. Hahn, *Chem. Rev.* **2018**, *118*, 9455–9456; d) A. Feliciano, J. L. Vázquez, L. J. Benítez-Puebla, I. Velazco-Cabral, D. C. Cruz, F. Delgado, M. A. Vázquez, *Chem. Eur. J.* **2021**, *27*, 8233–8251.
- [3] K.-S. Feichtner, V. H. Gessner, *Chem. Commun.* **2018**, *54*, 6540–6553.
- [4] For examples, see: a) D. V. Gutsulyak, W. E. Piers, J. Borau-Garcia, M. Parvez, *J. Am. Chem. Soc.* **2013**, *135*, 11776–11779; b) R. M. Brown, J. Borau-Garcia, J. Valjus, C. J. Roberts, H. M. Tuononen, M. Parvez, R. Roesler, *Angew. Chem. Int. Ed.* **2015**, *54*, 6274–6277; *Angew. Chem.* **2015**, *127*, 6372–6375.
- [5] R. J. Somerville, J. Campos, *Eur. J. Inorg. Chem.* **2021**, 3488–3498.
- [6] a) R. C. Fischer, P. P. Power, *Chem. Rev.* **2010**, *110*, 3877–3923; b) P. P. Power, *Nature* **2010**, *463*, 171–177; c) T. J. Hadlington, M. Driess, C. Jones, *Chem. Soc. Rev.* **2018**, *47*, 4176–4197.
- [7] H. Hashimoto, K. Nagata, *Chem. Lett.* **2021**, *50*, 778–787.
- [8] a) P. M. Keil, T. Szilvasi, T. J. Hadlington, *Chem. Sci.* **2021**, *12*, 5582–5590; b) P. M. Keil, T. J. Hadlington, *Angew. Chem. Int. Ed.* **2022**, *61*, e202114143; *Angew. Chem.* **2022**, *134*, e202114143.
- [9] M. Beller, *Chem. Rev.* **2019**, *119*, 2089–2089.
- [10] See the below, and references therein: S. M. Rummelt, P. O. Peterson, H. Zhong, P. J. Chirik, *J. Am. Chem. Soc.* **2021**, *143*, 5928–5936.
- [11] R. Arevalo, P. J. Chirik, *J. Am. Chem. Soc.* **2019**, *141*, 9106–9123.
- [12] a) T. Zell, D. Milstein, *Acc. Chem. Res.* **2015**, *48*, 1979–1994; b) R. P. Yu, J. M. Darmon, S. P. Semproni, Z. R. Turner, P. J. Chirik, *Organometallics* **2017**, *36*, 4341–4343.
- [13] a) T. A. Schmedake, M. Haaf, B. J. Paradise, A. J. Millevolte, D. R. Powell, R. West, *J. Organomet. Chem.* **2001**, *636*, 17–25; b) H. Tobita, A. Matsuda, H. Hashimoto, K. Ueno, H. Ogino, *Angew. Chem. Int. Ed.* **2004**, *43*, 221–224; *Angew. Chem.* **2004**, *116*, 223–226; c) H. P. Hickox, Y. Wang, Y. Xie, M. Chen, P. Wei, H. F. Schaefer III, G. H. Robinson, *Angew. Chem. Int. Ed.* **2015**, *54*, 10267–10270; *Angew. Chem.* **2015**, *127*, 10405–10408; d) M. M. Hänninen, K. Pal, B. M. Day, T. Pugh, R. A. Layfield, *Dalton Trans.* **2016**, *45*, 11301–11305; e) P. W. Smith, T. D. Tilley, *J. Am. Chem. Soc.* **2018**, *140*, 3880–3883.
- [14] a) P. B. Hitchcock, M. F. Lappert, S. A. Thomas, A. J. Thorne, A. J. Carty, N. J. Taylor, *J. Organomet. Chem.* **1986**, *315*, 27–44; b) T. Ochiai, D. Franz, X.-N. Wu, S. Inoue, *Dalton Trans.* **2015**, *44*, 10952–10956; c) T. P. Dhungana, H. Hashimoto, H. Tobita, *Dalton Trans.* **2017**, *46*, 8167–8179.
- [15] a) M. Weidenbruch, A. Stilter, K. Peters, H. G. Von Schnering, *Chem. Ber.* **1996**, *129*, 1565–1567; b) M. Weidenbruch, A. Stilter, W. Saak, K. Peters, H. G. Von Schnering, *J. Organomet. Chem.* **1998**, *560*, 125–129; c) J. J. Schneider, N. Czap, D. Bläser, R. Boese, *J. Am. Chem. Soc.* **1999**, *121*, 1409–1410; d) J. J. Schneider, N. Czap, D. Bläser, R. Boese, J. Ensling, P. Gütlich, C. Janiak, *Chem. Eur. J.* **2000**, *6*, 468–474; e) S. M. Mansell, R. H. Herber, I. Nowik, D. H. Ross, C. A. Russell, D. F. Wass, *Inorg. Chem.* **2011**, *50*, 2252–2263; f) H. Zhao, J. Li, X. Xiao, M. Kira, Z. Li, T. Müller, *Chem. Eur. J.* **2018**, *24*, 5967–5973.
- [16] H. Lei, J.-D. Guo, J. C. Fettinger, S. Nagase, P. P. Power, *Organometallics* **2011**, *30*, 6316–6322.
- [17] R. C. Handford, M. A. Nesbit, P. W. Smith, R. D. Britt, T. D. Tilley, *J. Am. Chem. Soc.* **2022**, *144*, 358–367.
- [18] M. Widemann, K. Eichele, H. Schubert, S. P. Sindlinger, S. Klenner, R. Pöttgen, L. Wesemann, *Angew. Chem. Int. Ed.* **2021**, *60*, 5882–5889; *Angew. Chem.* **2021**, *133*, 5946–5953.
- [19] P. M. Keil, T. J. Hadlington, *Chem. Commun.* **2022**, *58*, 3011–3014.
- [20] a) J. Cheng, J. Liu, X. Leng, T. Lohmiller, A. Schnegg, E. Bill, S. Ye, L. A. Deng, *Inorg. Chem.* **2019**, *58*, 7634–7644; b) J. Cheng, Q. Chen, X. Leng, S. Ye, L. Deng, *Inorg. Chem.* **2019**, *58*, 13129–13141.
- [21] Y. Liu, J. Cheng, L. Deng, *Acc. Chem. Res.* **2020**, *53*, 244–254.
- [22] P. M. Keil, T. J. Hadlington, *Z. Anorg. Allg. Chem.* **2022**, e202200141.
- [23] These are stabilized by the  $[\text{BAR}^{\text{F}}_4]^-$  counter anion ( $\text{Ar}^{\text{F}} = 3,5\text{-(CF}_3)_2\text{C}_6\text{H}_3$ ).
- [24] Deposition numbers 2202847, 2202848, 2202849, 2202850, 2202851, 2202852, and 2202853 contain the supplementary crystallographic data for this paper. These data are provided free of charge by the joint Cambridge Crystallographic Data Centre and Fachinformationszentrum Karlsruhe Access Structures service.
- [25] a) B. Blom, G. Tan, S. Enthaler, S. Inoue, J. D. Epping, M. Driess, *J. Am. Chem. Soc.* **2013**, *135*, 18108–18120; b) M.-P. Luecke, D. Porwal, A. Kostenko, Y.-P. Zhou, S. Yao, M. Keck, C. Limberg, M. Oestreich, M. Driess, *Dalton Trans.* **2017**, *46*, 16412–16418.
- [26] We note that the remainder of aromatic signals, including those relating to the “free” Dipp group of the NHC ligand, are found as broad signal in the usual region, between 6.9 and 8.0 ppm.
- [27] A. Bondi, *J. Phys. Chem.* **1964**, *68*, 441–451.
- [28] a) S. Hino, M. Brynda, A. D. Philips, P. P. Power, *Angew. Chem. Int. Ed.* **2004**, *43*, 2655–2658; *Angew. Chem.* **2004**, *116*, 2709–2712; b) J. Li, S. Schenk, F. Winter, H. Scherer, N. Trapp, A. Higelin, S. Keller, R. Pöttgen, I. Krossing, C. Jones, *Angew. Chem. Int. Ed.* **2012**, *51*, 9557–9561; *Angew. Chem.* **2012**, *124*, 9695–9699.
- [29] a) B. N. Figgis, *Nature* **1958**, *182*, 1568–1570; b) S. C. Coste, T. J. Pearson, D. E. Freedman, *Inorg. Chem.* **2019**, *58*, 11893–11902.
- [30] Derived through DFT calculations. See Supporting Information for details.
- [31] For examples of our earlier endeavours here, see refs. [8] and [19].
- [32] a) J. Zhao, A. S. Goldman, J. F. Hartwig, *Science* **2005**, *307*, 1080–1082; b) J. I. var der Vlugt, *Chem. Soc. Rev.* **2010**, *39*, 2302–2322.
- [33] From these mixtures, only very small amounts of the iron(II) amide compound,  $^{\text{PhIP}}\text{DippFeNH}_2$ , could be isolated, formed presumably through a complex ligand redistribution reaction.
- [34] a) A. Meltzer, S. Inoue, C. Präsang, M. Driess, *J. Am. Chem. Soc.* **2010**, *132*, 3038–3046; b) T. J. Hadlington, T. Szilvasi, M. Driess, *J. Am. Chem. Soc.* **2019**, *141*, 3304–3314.
- [35] Compound **6** isolated in this way always formed as a mixture with **4**, which could not be separated.
- [36] U. Schubert, S. Gilbert, S. Mock, *Chem. Ber.* **1992**, *125*, 835–837.
- [37] a) Y. Wakatsuki, K. Aoki, H. Yamazaki, *J. Am. Chem. Soc.* **1974**, *96*, 5284–5287; b) R. G. Teller, R. G. Finke, J. P. Collman, H. B. Chin, R. Ban, *J. Am. Chem. Soc.* **1977**, *99*, 1104–

- 1111; c) W. W. Brennessel, R. E. Jilek, J. E. Ellis, *Angew. Chem. Int. Ed.* **2007**, *46*, 6132–6136; *Angew. Chem.* **2007**, *119*, 6244–6248.
- [38] For selected examples, see: a) C. Mahon, W. L. Reynolds, *Inorg. Chem.* **1967**, *6*, 1927–1928; b) P. Le Floch, F. Knoch, F. Kremer, F. Mathey, J. Scholz, W. Scholz, K.-H. Thiele, U. Zenneck, *Eur. J. Inorg. Chem.* **1998**, 119–126; c) C. Lichtenberg, L. Viciu, M. Adelhardt, J. Sutter, K. Meyer, B. de Bruin, H. Grutzmacher, *Angew. Chem. Int. Ed.* **2015**, *54*, 5766–5771; *Angew. Chem.* **2015**, *127*, 5858–5863; d) T. M. Maier, M. Gawron, P. Coburger, M. Bodensteiner, R. Wolf, M. P. van Leest, B. de Bruin, S. Demeshko, *Inorg. Chem.* **2020**, *59*, 16035–16052.
- [39] a) M.-E. Moret, J. C. Peters, *Angew. Chem. Int. Ed.* **2011**, *50*, 2063–2067; *Angew. Chem.* **2011**, *123*, 2111–2115; b) M. E. Moret, J. C. Peters, *J. Am. Chem. Soc.* **2011**, *133*, 18118–18121; c) G. Ung, J. C. Peters, *Angew. Chem. Int. Ed.* **2015**, *54*, 532–535; *Angew. Chem.* **2015**, *127*, 542–545.
- [40] We note that the CV of **3** shows a relatively large peak separation,  $\Delta E_p$ , which is most likely due to the high concentration of this sample (3 mM). To corroborate this, a 3 mM ferrocene sample was run under identical conditions, also giving a large  $\Delta E_p$  of 234 mV (see Figure S59 in Supporting Information).
- [41] N. G. Connelly, W. E. Geiger, *Chem. Rev.* **1996**, *96*, 877–910.
- [42] This would suggest that the reduced species has some degree of stability at ambient temperature on the timescale of the CV experiments (e.g. minutes). However, due to challenges in generating and isolating this species through reduction using chemical methods, the  $\text{Ge}^{\text{II}}\text{-Fe}^{-\text{I}}$  species (*viz.* **7**) could not be accessed in our hands.
- [43] Spectrum referenced to a  $\text{Mn}^{2+}$  standard, see Supporting Information for details.
- [44] a) M. J. Therien, W. C. Trogler, *J. Am. Chem. Soc.* **1986**, *108*, 3697–3702; b) R. Gilbert-Wilson, L. D. Field, S. B. Colbran, M. M. Bhadbhade, *Inorg. Chem.* **2013**, *52*, 3043–3053; c) M. A. Nesbit, P. H. Oyala, J. C. Peters, *J. Am. Chem. Soc.* **2019**, *141*, 8116–8127.
- [45] a) A. G. Davies, D. Griller, B. P. Roberts, *J. Am. Chem. Soc.* **1972**, *94*, 1782–1783; b) B. Das, A. Makol, S. Kundu, *Dalton Trans.* **2022**, *51*, 12404–12426; c) A. Sekiguchi, T. Fukawa, V. Ya Lee, M. Nakamoto, *J. Am. Chem. Soc.* **2003**, *125*, 9250–9251; d) T. Y. Lai, L. Tao, R. D. Britt, P. P. Power, *J. Am. Chem. Soc.* **2019**, *141*, 12527–12530.
- [46] P. Gütllich, E. Bill, A. X. Trautwein, *Mössbauer Spectroscopy and Transition Metal Chemistry*, Springer-Verlag, Berlin, Heidelberg, **2011**.

Manuscript received: December 8, 2022

Accepted manuscript online: February 9, 2023

Version of record online: March 22, 2023